Elastic scattering of π^+ and π^- from ^{4}He between 90 and 240 MeV

B. Brinkmöller,[a] C. L. Blilie,[b] D. Dehnhard, M. K. Jones,[c] G. M. Martinez,

S. K. Nanda,[d] S. M. Sterbenz,[e] and Yi-Fen Yen
University of Minnesota, Minneapolis, Minnesota 55455

L. G. Atencio, S. J. Greene, C. L. Morris, and S. J. Seestrom
Los Alamos National Laboratory, Los Alamos, New Mexico 87545

G. R. Burleson, K. S. Dhuga,[f] J. A. Faucett, and R. W. Garnett[e]
New Mexico State University, Las Cruces, New Mexico 88003

K. Maeda
Tohoku University, Sendai, Japan

C. Fred Moore, S. Mordechai,[g] A. Williams,[h] and S. H. Yoo[e]
University of Texas, Austin, Texas 78712

L. C. Bland[i]
University of Pennsylvania, Philadelphia, Pennsylvania 19104
(Received 6 June 1991)

In a series of experiments, differential cross sections for elastic scattering of π^+ and π^- from ^{4}He were measured at the Clinton P. Anderson Meson Physics Facility (LAMPF). Data were taken at incident energies between T_π= 90 and 240 MeV using different experimental setups which covered the angular range from far forward ($\approx 10°$) to far backward angles ($\approx 170°$). A phase-shift analysis of the data was carried out. The experimental phase shifts are compared with values predicted by a first-order optical model program.

I. INTRODUCTION

Pion scattering from ^{4}He is well suited for a test of pion-nucleus interaction models because the wave function of ^{4}He, with spin and isospin being equal to zero, is simple. Therefore, most theoretical analyses [1–7] of pion scattering on nuclei, undertaken with the aim to improve microscopic optical models, have first been tested on ^{4}He. A review of the different approaches has been given by Thomas and Landau [8].

Due to its small size, fewer partial waves contribute to the scattering from ^{4}He than from heavier nuclei, which facilitates the theoretical analysis in terms of the free pion-nucleon force. Because of evidence that pions penetrate into regions of higher density in scattering from ^{4}He than from heavier nuclei, higher-order terms are expected to be relatively important. Thus, a set of precise π-^{4}He elastic-scattering data should allow a detailed study of this simple pion-nucleus system, including second-order effects. A new effort in understanding ^{4}He (π, π) elastic scattering is also warranted since the charge density of the ground state of ^{4}He is now well determined from precise electron-scattering data [9] over a large range of momentum transfer from q = 0.14 to 7.7 fm^{-1}.

In the energy interval between T_π = 25 and 75 MeV, differential cross sections have been measured by Nordberg and Kinsey [10], Crowe *et al.* [11], and Fournier *et al.* [12]. The most extensive data set of π^- scattering was obtained by Binon *et al.* [13] at incident energies between T_π = 110 and 260 MeV. Data between 68 and 204 MeV were also taken for both pion polarities by Shcherbakov *et al.* [14]. At slightly higher energies, data were obtained by Källne *et al.* [15] between 260 and 310 MeV and by Boswell *et al.* [16] between 300 and 475 MeV. There has been, for some time, a need for good quality π^+ data at all energies and for better statistics π^- data at large angles in the energy region of the P_{33} resonance.

We have made use of the high-quality pion beams provided at the Clinton P. Anderson Meson Physics Facility (LAMPF) in order to obtain the data that are necessary for an unambiguous determination of the pion-nucleus phase shifts. Such a set of phase shifts should give new insights into the shortcomings of models which have been developed thus far to describe the interaction of pions with nuclei. The ultimate goal is to understand the modifications of the free pion-nucleon force in the nuclear medium.

II. THE EXPERIMENT

A. General remarks on setups and target

The data were taken with the high-resolution Energetic Pion Channel and Spectrometer (EPICS) [17] at LAMPF. The incident energies were chosen between T_π = 90 and 240 MeV to cover the region of the P_{33} pion-nucleon resonance.

Two different experimental setups were employed in a series of measurements to cover the angular range from $\Theta_{lab} = 10°$ to about 165° at most energies. For the intermediate range, 30° to 120°, and the far forward angles, 10° to 30°, the standard EPICS setup was used. At far forward angles the muon halo of the incident beam contributed a large background to the spectra which required a nonstandard method of normalization (see below). For the measurements between $\approx$ 115° and 165° the EPICS large-angle setup was employed with the target placed inside the field of a dipole magnet [18].

As usual in experiments with the EPICS system, the absolute differential cross sections for ^{4}He(π,π) were determined by normalizing the π + ^{4}He yields to π + p yields measured under essentially the same conditions. The normalization factor is the ratio of the π + p cross section, calculated from existing phase shifts [20], to the π + p yields measured in this experiment. The uncertainties in the phase shifts cause an overall uncertainty in the absolute cross sections of < 4%, depending on the incident energy and the angle at which the π + p measurements were done. Some details of the setups and the normalization runs are discussed in the next three subsections.

A gas target was used both for the ^{4}He measurements and for the normalization runs using $^1H_2$ or CH_4 as the target material. The target container was a cylindrical flask of 12.7-cm diameter with walls of 25-μm-thick stainless-steel foils. The symmetry axis of the flask was perpendicular to the reaction plane. When filled with ^{4}He, the target was cooled to a temperature of about 20 K at a pressure of 1.4 bars. When filled with hydrogen gas, the temperature was about 40 or 80 K at several different pressures. The measurements on CH_4 were done at room temperature (at $\approx$ 1.6 bars) which has the advantage of avoiding possible condensation of water on the target window.

B. Measurements at intermediate angles

Spectra were taken [19] at T_π = 90, 110, 130, 150, and 180 MeV for π^+ scattering between 30° and 120° mostly in 5° steps. For π^-, data were taken at 150 and 180 MeV for comparison with the data of Binon *et al.* [13]. Additional data were obtained for both π^+ and π^- at 240 MeV.

The normalization runs with hydrogen were done at all energies at a laboratory angle of 30°, except at 90 MeV where $\Theta_{lab} = 40°$ was used. Because of the large diameter of the gas target, the amount of target volume that is within the acceptance of the spectrometer changes with angle. To attain the angular dependence of the normalization factor, yields for scattering from hydrogen were measured at all angles at T_π = 110 and 180 MeV.

The magnetic fields of the spectrometer were adjusted for each run to place the elastically scattered pions from ^{4}He and those scattered from ^{1}H at the same position in the focal plane of the spectrometer. This minimizes the effects of the difference in the momenta of pions scattered by ^{4}He and ^{1}H, on the effective solid angle.

The angular acceptance of EPICS, which is about 5°, was subdivided into smaller bins to obtain the angular resolution necessary to determine the details of the angular distributions. When the binning was done on the scattering angle calculated from the particle's trajectories, differences between the effective solid angles for scattering from the two nuclei still exist. The differences are largest at the edges of the angular acceptance, due to the large difference in $dT_\pi/d\Theta_{lab}$ for pions scattered from the two nuclei. However, when the angular acceptance of the spectrometer was subdivided by binning the position spectra from the front wire chambers instead of applying the bins to the calculated scattering angles, the effective solid angle of each bin was the same, for both the ^{1}H and ^{4}He measurements. This procedure resulted in a minor loss of angular resolution. Five bins were obtained, with a spacing of about 1° and a width of about 1.5° each.

C. Measurements at backward angles

For the large-angle measurements the target was placed at the center of the circular dipole magnet EURYDICE [18]. This magnet bends the particles scattered at large angles to floor angles that can be reached by the spectrometer. Here, "floor angle" refers to the nominal scattering angle used in measurements without EURYDICE. In this setup the spectrometer is displaced horizontally with respect to an axis passing through the center of EURYDICE by a fixed offset, and the target position is displaced with respect to the pion channel axis by a variable offset D. To obtain the desired scattering angle for particles of a certain momentum, the magnetic field of the EURYDICE magnet, the offset D, and the floor angle of the spectrometer have to be adjusted.

These variables were calculated for scattering events at the center of the magnetic field. Originally, an effective-field-boundary (EFB) approximation was used to determine the bending angle for the incoming and outgoing trajectories. The effective radius R of the magnetic field had been determined by a floating wire measurement of an offset D using the relation $D = R^2/(2\rho)$, where ρ is the radius of curvature of the wire inside the field (see Figs. 2 and 3 in Ref. [18]).

We observed systematic differences between the calculated scattering angles, using the radius R from the floating wire measurement, and the scattering angles deduced from the measured pion energy. There was also a normalization problem near $\Theta_{lab} = 120°$ between the data taken at intermediate and at large angles. Both of these problems were traced to the fact that the floating wire measurements had produced values of R that were systematically too large. This error occurs because the rela-

tion linking R and D is only a very crude approximation that systematically gives too large values of R, especially for magnets with large fringing fields. Therefore a field map of the EURYDICE magnet was obtained [21]. A Monte Carlo program was written by one of us (B.B.) to calculate the scattering angle using ray-trace algorithms. The scattering angles obtained with this program were found to be in good agreement with angles determined from the energy measurement.

The Monte Carlo calculations also showed that the acceptance of EPICS in the large-angle setup for ^{4}He(π,π) is slightly different from the acceptance for the ^{1}H(π,π) measurements that were used for normalization. This finding resolved the discrepancy between the absolute cross sections near $\Theta_{\rm lab} = 120°$ from the measurements at intermediate and large angles. During a subsequent run, this overlap region was measured again. The results confirmed the predictions of the Monte Carlo calculations.

Because the location of the scattering event within the gas target cannot be reconstructed from the trajectory of the outgoing pion, the path lengths of both the outgoing and incoming pion within the magnetic field of the EURYDICE magnet are uncertain. This introduces an uncertainty in the calculated scattering angle and thus reduces the angular resolution of the system. Therefore, the angular acceptance was not subdivided for the measurements with the large-angle setup. This was not of a disadvantage because the measured angular distributions do not suggest any sharp structures at large angles.

For π^+, spectra were taken during these large-angle measurements between $\Theta_{\rm lab} \approx 116°$ and 166° in 5° steps at six energies between 90 and 240 MeV. For π^-, data were obtained at 150 and 180 MeV at the same angles and at 240 MeV at only two angles. Normalization runs with hydrogen were done at $\approx$ 156° at all energies and the angle dependence of the normalization was obtained from the Monte Carlo calculations.

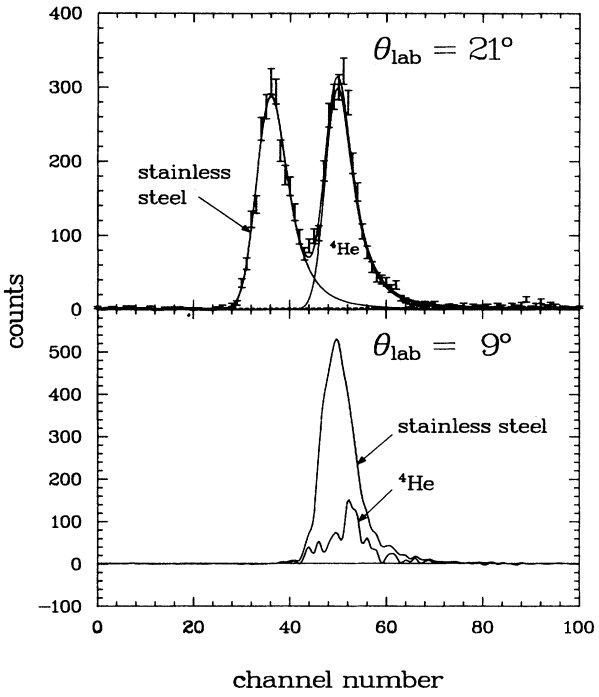

FIG. 1. Missing-mass spectra from cooled gas target at the incident energy T_π = 110 MeV at $\Theta_{\rm lab}$ = 21° (a) and 9° (b). The pions elastically scattered from ^{4}He are clearly separated from the pions scattered from the stainless steel of the target walls at 21°. At 9° an empty-target spectrum is shown and the result of subtracting the empty-target from the full-target spectrum.

D. Measurements at far forward angles

The measurements for π scattering from ^{4}He at far forward angles were done both for π^+ and π^- at 110, 130, 150, 180, and 240 MeV, starting at $\Theta_{\rm lab} = 30°$, in 3° or 2° steps. For angles larger than or equal to 21°, the energy resolution of EPICS was sufficient to resolve pions elastically scattered by ^{4}He from those scattered by the target walls (Fig. 1). For smaller angles, empty-target runs were taken for background subtraction. Uncertainties in reproducing the scattering angle used in the ^{4}He measurement for the empty-target runs introduced a systematic uncertainty of up to 20% below $\Theta_{\rm lab} = 21°$.

At far forward angles the efficiency of the EPICS system is reduced because of a large number of double hits in the front wire chambers of the spectrometer. (For these double hits it is impossible to reconstruct the trajectory of the measured particles.) The standard method to measure the efficiency of the EPICS spectrometer includes an angle consistency check between the trajectory angles measured by the front and the rear wire chambers of the spectrometer. It was found that this procedure introduced a large uncertainty in the efficiency, especially when the spectrometer is operated within the muon halo of the beam. This uncertainty was avoided by using information primarily from the rear chambers where the counting rates are small.

Angular distributions for π^+ scattering beyond about 18° were measured with standard slit settings in the EPICS channel. For measurements at angles less than 18° the slits were narrowed considerably to reduce the pion flux by about a factor of 10. In addition, slits located directly before the front wire chambers of the spectrometer were used to reduce the count rate from the muon halo of the beam. With these slit settings it was possible to take angular distributions forward to about 9° before the efficiency dropped below 50%. Because of the lower incident beam flux for π^- scattering, the angular distribution could be measured forward to about 11° with standard slit settings before the efficiency dropped below 50%. Attempts to take data with efficiencies below 50% gave unacceptably large uncertainties. For this set of forward-angle measurements, normalization runs were done at 30° at all energies, and between 13° and 30° at T_π = 180 MeV.

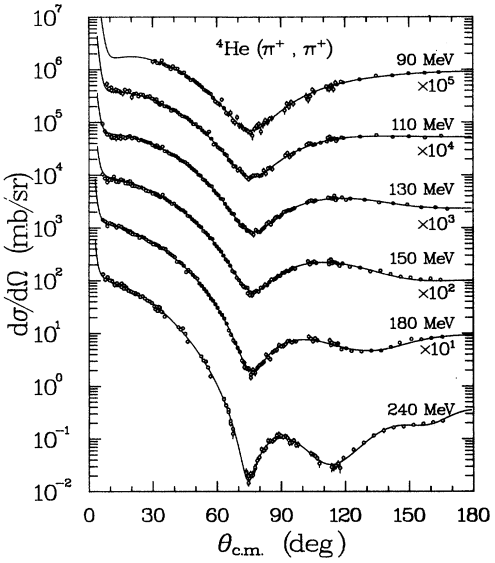

FIG. 2. Angular distributions for ^{4}He(π^+, π^+) elastic scattering between T_π = 90 and 240 MeV. The solid lines are results of phase-shift fits of the data.

E. Experimental results

An overview of the measured angular distributions is given in Fig. 2 for ^{4}He(π^+, π^+) scattering and in Fig. 3 for ^{4}He(π^-, π^-) scattering. The data taken with the different setups were independently analyzed and normalized. The overlap of the three data sets near 120° and at 30° is excellent. The solid lines in the plots are results of phase-shift analyses that are described in Sec. III B.

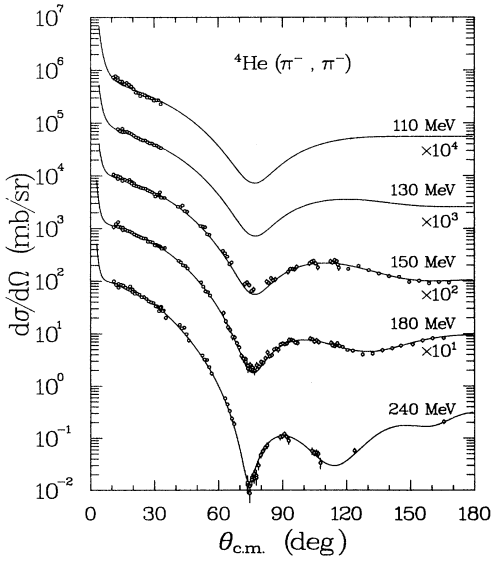

FIG. 3. Angular distributions for ^{4}He(π^-, π^-) elastic scattering between 110 and 240 MeV. The solid lines are results of phase-shift fits of the data.

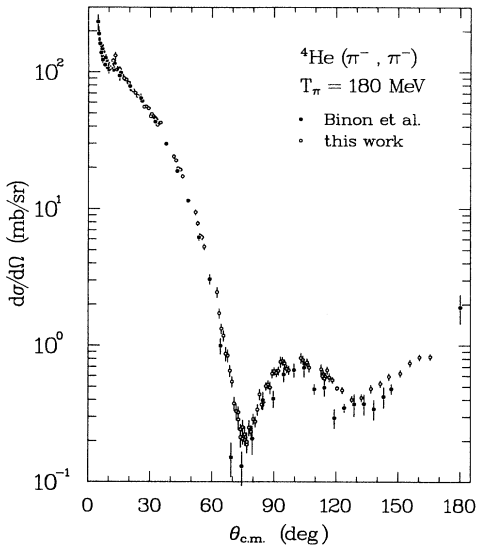

FIG. 4. Angular distribution for ^{4}He(π^-, π^-) at T_π = 180 MeV from this experiment and from Binon *et al.* [13].

In Fig. 4 our data are compared to the data of Binon *et al.* [13] for ^{4}He(π^-, π^-) scattering at T_π = 180 MeV. The two data sets are in good agreement with each other in the small angle region. However, for angles between 60° and 170° the data of Ref. [13] are systematically lower than our measurement. This might be due to a small (a few MeV) difference between the incident pion energies of the two experiments. An extrapolation of our large-angle measurements to 180° suggests a value of ≈ 0.9 mb/sr, which is less than half the value of Binon *et al.* [13] who had detected the recoiling ^{4}He nucleus at 0° to determine the cross section at 180°. It is likely that this recoil measurement suffered from a normalization problem. Our phase-shift analysis (see Sec. III B below) also supports an extrapolation to a value of about 0.9 mb/sr.

Because of the good statistics in the present data, the position and the depth of the minimum in the angular distribution near 75° are quite well determined. At small angles Binon's data extend further into the far forward region than ours. In the angle region covered by our data, there now exist both π^+ and π^- cross sections. This allows more stringent tests of theoretical predictions than were previously possible with data for one pion polarity alone.

III. ANALYSIS OF THE DATA

A. Optical model analysis

It is beyond the scope of this work to test the most advanced theoretical approaches used to calculate a microscopic optical potential. Instead, we have attempted to gain some insight into the qualitative behavior of the pion-nucleus interaction by a comparison of best-fit pion-nucleus phase shifts extracted from our data, to predic-

tions of a relatively simple model employed in the computer program PIPIT [22]. This program uses the factorization approximation to calculate the first-order optical potential $U(\mathbf{k},\mathbf{k}')$ from the properties of the nuclear ground state and the t matrix of the π-N system:

$$U(\mathbf{k},\mathbf{k}') = \frac{A-1}{A}\,[\,\rho_p(\mathbf{q})\cdot t_{\pi p}(\mathbf{k}',\mathbf{k};\mathbf{k}_0) + \rho_n(\mathbf{q})\cdot t_{\pi n}(\mathbf{k}',\mathbf{k};\mathbf{k}_0)]\,. \quad (1)$$

Here $\mathbf{k}$ ($\mathbf{k}'$) is the incident (outgoing) π-nucleus momentum in the center of mass and $\mathbf{k}_0$ is the total on-shell ($|\,\mathbf{k}'\,|=|\,\mathbf{k}\,|=|\,\mathbf{k}_0\,|$) momentum in the π-nucleus center of mass. A is the number of target nucleons, $\mathbf{q}$ the momentum transfer, $\rho_p(\mathbf{q})$ [$\rho_n(\mathbf{q})$] the Fourier transform of the ground-state proton [neutron] point density, and $t_{\pi p}$ ($t_{\pi n}$) the π-proton (π-neutron) effective interaction which is constructed from the $T=\frac{1}{2}$ and $T=\frac{3}{2}$ isospin components of the free π-nucleon t-matrix.

The free π-nucleon t matrices were derived from the phase shifts of Arndt [20]. The optical potential U needs to be calculated for off-shell kinematics which means that $t_{\pi p}$ and $t_{\pi n}$ are needed off-shell ($|\,\mathbf{k}'\,|\neq|\,\mathbf{k}\,|=|\,\mathbf{k}_0\,|$). Because the off-shell π-N t matrix cannot be obtained from π-N scattering data, it must be estimated from a theoretical model. Numerous models have been applied for this off-shell extrapolation [3–8]. In most cases, separable potentials have been used [23]. It has been found that the range of the elementary π-N interaction used to construct these potentials has a large effect on the results of the calculated cross sections [3, 5, 8].

In PIPIT the off-shell t matrix is calculated using

$$t_l(\mathbf{k},\mathbf{k}') = t_l(\mathbf{k}_0)\frac{g_l(\mathbf{k})g_l(\mathbf{k}')}{g_l^2(\mathbf{k}_0)}, \quad (2)$$

where l is the orbital angular momentum in the π-N system and g_l is an off-shell Gaussian damping factor,

$$g_l = k^l \exp(-a_l k^2), \quad (3)$$

which is employed for both the $l=0$ and $l=1$ partial waves. The parameters a_l, which are related to the π-N interaction range, were treated as free parameters to fit the data. We chose $a_{l=0} = a_{l=1} = 5\times10^{-6}$ (MeV/c)$^{-2}$, which is consistent with reasonable values of the interaction range [3].

There have been several studies on the choice of the energy at which the π-N t matrices in Eq. (1) should be evaluated [4, 6, 7]. Because of binding energy effects and Fermi motion the relation of this energy to the incident pion energy is not simple. Theoretical estimates [4, 7] suggest that good results can be achieved if the pion-nucleon energy is evaluated at an energy which is lower than the incident energy by ΔE of up to about 20 MeV. This energy shift depends on the incident pion energy. In our analysis we used ΔE as a fit parameter. The best fits to the data were obtained with $\Delta E = (T_\pi + 10\ \text{MeV})/10$ for pion energies below 170 MeV and a constant value of 18 MeV for the higher energies. This prescription is not unreasonable in comparison with theory [4, 7] and fits data on a variety of nuclei [24].

The nucleon point densities needed for the optical potential in Eq. (1) were deduced from elastic electron-scattering data [9]. The proton and neutron point densities were assumed to have the same shape. To calculate this nucleon point density for ^{4}He the individual proton and neutron charge densities were unfolded numerically from the experimentally measured charge distribution [9] using the programs ALLWORLD [25] and UNFOLD [26]. The nucleon charge distributions [27] were assumed to have a Gaussian shape with a mean square radius of $\langle r_p^2\rangle = 0.64$ fm^2 for the proton and $\langle r_n^2\rangle = -0.12$ fm^2 for the neutron.

The nucleon point density in momentum space, deduced from the measured charge density, differs from that of a simple Gaussian shape (of the same rms radius) beyond $q = 2.2$ fm^{-1}, and it becomes negative for $q \geq 3.1$ fm^{-1}. The effect of these density differences on the differential cross sections [28] are significant only at our highest energies at large angles (momentum transfers beyond $q \approx 2.2$ fm^{-1}).

The PIPIT predictions for ^{4}He(π^+,π^+) elastic scattering at $T_{\pi+} = 90$, 110, 130, 150, 180, and 240 MeV, using the above-mentioned point densities, are shown in Fig. 5. The general trend of the data is reproduced quite well by the calculated cross sections. However, there are some significant discrepancies:

(1) At 110 MeV the calculated ^{4}He(π^+,π^+) angular distribution near $\Theta_{\text{c.m.}} = 10°$ shows a distinct minimum due to destructive Coulomb-nuclear interference which is not seen in the experimental cross sections. Similarly, for ^{4}He(π^-,π^-), constructive interference leads to *larger* calculated cross sections (not shown) than observed in this angular range. These discrepancies may be linked to the neglect of true pion absorption. Pion absorption affects mainly the imaginary part of the nuclear amplitude

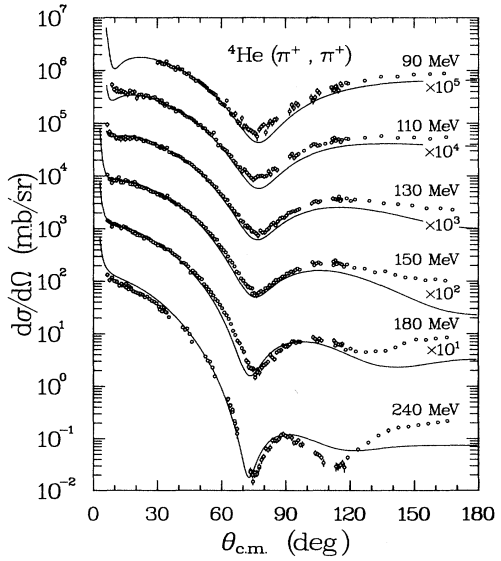

FIG. 5. Angular distributions for ^{4}He(π^+,π^+) from this experiment and predictions of optical model calculations using the program PIPIT [22].

which does not interfere with the Coulomb amplitude. True pion absorption has been found to contribute significantly to ^{4}He(π,π) scattering at lower energies [4, 7, 8].

(2) At all energies the slope of the calculated angular distribution between $\Theta_{\text{c.m.}} = 30°$ and the first minimum at $\Theta_{\text{c.m.}} \approx 75°$ is too steep in comparison with the data. At lower energies the predicted cross sections in the minimum are too low, whereas at higher energies the position of the minimum is predicted at too small an angle. This is an indication (which is verified by our phase-shift analysis) that the optical model calculation predicts larger contributions from higher partial waves than the data require.

(3) The predicted cross sections at large angles are generally smaller than the experimental ones. It has been shown that the inclusion of a ρ^2 term in the optical potential to account for nucleon-nucleon correlations tends to increase the cross sections at large angles [3, 6, 7].

In order to investigate whether the observed discrepancies are indeed due to the proposed effects, studies are currently under way using more advanced optical models [29, 30].

B. Phase-shift analysis

Partial-wave analyses have been carried out previously on ^{4}He(π,π) data [13, 31, 32]. Some of these data are only for π^-, others cover only limited ranges of angles. The present measurements provide detailed data over a large range of angles at many energies for π^+ and not quite as extensive data for π^- (which supplement the data of Binon [13]). This data set should allow a study of systematic trends in the phase shifts, δ_l^{Re} and δ_l^{Im}.

The program PAW [19] was used to search on δ_l^{Re} and $\eta_l = \exp(-2\delta_l^{\text{Im}})$ to fit the measured differential cross sections. This code uses subroutines from the MINUIT [33] package in fitting the phase shifts by minimizing χ^2. The Coulomb phases were calculated for the field of a point charge. A simultaneous fit to both ^{4}He(π^+,π^+) and ^{4}He(π^-,π^-) data was performed assuming charge symmetry of the strong interaction.

The differences between π^+ and π^- scattering in the region of Coulomb–nuclear interference are made more apparent in Fig. 6, which shows the angular distributions only at the forward angles. An accurate measurement of the cross sections in this region is crucial for the determination of the real and imaginary parts of the amplitude and the extrapolation of the amplitudes to $\Theta = 0°$.

In this angular region the cross sections for π^- scattering are larger than those for π^+ scattering at energies below the resonance. The differences decrease rapidly from $T_\pi = 110$ to $T_\pi = 180$ MeV. For $T_\pi = 240$ MeV, the differences remain small; however, the partial-wave analysis gives a slightly *smaller* cross section for π^- scattering than for π^+ scattering.

The number of partial waves that contribute to the cross sections may be estimated from $l \approx 3kr$. Here k is the center-of-mass momentum and r is the rms radius of the nuclear density which is ≈ 1.7 fm for ^{4}He. For the highest energy, $T_\pi = 240$ MeV, $k = 1.7$ fm^{-1} which results in $l \approx 8$, whereas at the lowest energy, $T_\pi = 90$ MeV, $k = 0.9$ fm^{-1} which gives $l \approx 4$. It was found that partial waves up to $l = 6$ were needed at 240 MeV and partial waves up to $l = 3$ were sufficient at 90 MeV. Furthermore, the real part of the phase shift δ_l^{Re} for $l \geq 3$ proved to be small at all energies and could be fixed at $\delta_l^{\text{Re}} = 0$ without affecting the quality of the fits.

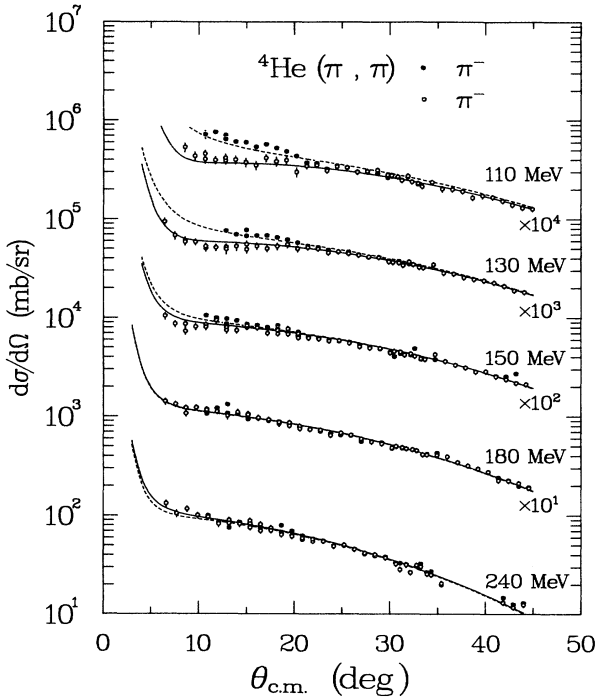

FIG. 6. Detail of the angular distributions for both ^{4}He(π^+,π^+) (open circles) and ^{4}He(π^-,π^-) (full circles) in the forward-angle region. The full lines are the result of the phase-shift analysis for π^+ scattering and the dashed lines the result for π^- scattering.

Some of the χ^2_{min} values obtained in fitting the data, assuming only statistical errors, were found to be quite large (see values in parentheses in Table I). Smaller values of χ^2_{min} were obtained by adding (in quadrature) to the statistical errors an uncertainty of 5% from the determination of the effective solid angle of the different angular bins into which the spectrometer acceptance had been subdivided.

A possible error of 20% due to a problem with reproducing the angle setting for the background subtraction measurements for angles smaller than 20° was not included in the fit. Also not included was the overall uncertainty of < 4% in absolute cross section due to the uncertainty in the knowledge of the $\pi + p$ elementary phase shifts [20].

The results of the phase-shift analysis are given in Table I. The fits give values for the reduced χ^2_{min} near 1 at most energies. The error quoted for each parameter corresponds to a change of χ^2_{min} to $\chi^2_{\text{min}} + 1$ keeping all other parameters at a fixed value.

In Figs. 7, 8, and 9, δ_l^{Re} and η_l for $l = 0$, 1, and 2, respectively, from the phase-shift fits are plotted as a function of the pion energy. Also shown are the results of the analysis of Binon *et al.* [13] and those obtained

TABLE I. Results of phase-shift analyses of the ^{4}He(π,π) elastic cross-section data. $\chi^2_{\min}$ denotes the minimum χ^2 per degree of freedom for the best fit. It was obtained after adding a 5% normalization error in quadrature to the statistical error of each data point (see text). The values in parentheses give the $\chi^2_{\min}$ without the additional normalization error. The errors quoted correspond to an increase of $\chi^2_{\min}$ by 1.

T_π (MeV)	$\chi^2_{\min}$	δ_0^{Re} (deg) η_0	δ_1^{Re} (deg) η_1	δ_2^{Re} (deg) η_2	η_3	η_4	η_5	η_6
90	0.99	−9.8±1.8	22.5±1.6	4.1±0.9				
	(1.88)	0.976±0.051	0.578±0.057	0.927±0.032	0.982±0.020			
110	1.36	−4.3±2.4	26.3±4.8	8.6±1.1				
	(3.97)	0.887±0.061	0.243±0.058	0.817±0.031	0.983±0.021	0.989±0.022		
130	0.69	−7.7±2.9	39.8±6.6	10.2±1.3				
	(2.19)	0.629±0.062	0.160±0.076	0.682±0.028	0.952±0.021	0.986±0.022		
150	1.81	−27.3±3.9	50.4±6.5	6.7±1.4				
	(7.78)	0.496±0.052	0.150±0.044	0.514±0.027	0.879±0.019	0.991±0.020	0.992±0.018	
180	1.03	−33.9±4.7	88.0±14.4	2.9±1.6				
	(3.85)	0.302±0.042	0.116±0.027	0.406±0.021	0.773±0.017	0.970±0.016	0.988±0.015	0.992±0.012
240	1.65	−47.3±3.0	157.4±22.6	−5.4±1.2				
	(6.10)	0.235±0.032	0.037±0.020	0.364±0.012	0.709±0.012	0.900±0.012	0.992±0.010	0.980±0.009

by Crowe *et al.* [11]. The low-energy values of Ref. [11] connect smoothly with ours and the results of Ref. [13]. One exception is η_0 where the values of Ref. [11] indicate too much absorption. An extrapolation of our analysis to lower energies indicates values near $\eta_0 = 1$ (no absorption) as expected. We note that it has been shown by Nichitiu and Sapozhnikov [34] that such a solution is, however, also consistent with the *data* of Ref. [11].

Generally our phase shifts compare well with Binon's [13], except for the $l = 1$ partial wave. There are significant differences in η_1 at 110 MeV and in δ_1^{Re} near 200 MeV. The latter occurs in a region where η_1 is very small so that δ_1^{Re} affects the cross sections only very little (because of strong absorption). The observed differences are mainly due to the tighter constraints on the phases because of the better statistics of our large-angle data.

The results of the phase-shift analysis for the individual l values can be compared in Figs. 7–9 with the results

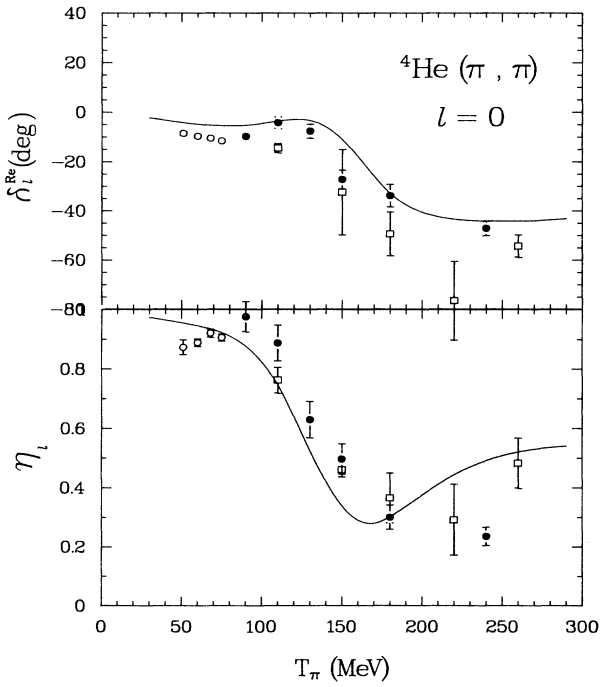

FIG. 7. Real phase shift $\delta^{\mathrm{Re}}_{l=0}$ and absorption coefficient $\eta_{l=0}$ for ^{4}He(π,π) as a function of pion energy. The full circles present the result of our phase-shift analysis, the open circles the results of Crowe *et al.* [11], and the open squares the results of Binon *et al.* [13]. The error bars correspond to a change in the reduced χ^2 of the fit to the measured cross section from $\chi^2_{\min}$ to $\chi^2_{\min} + 1$ keeping all other parameters of the fit at their optimum values. The line is the optical model prediction from this work.

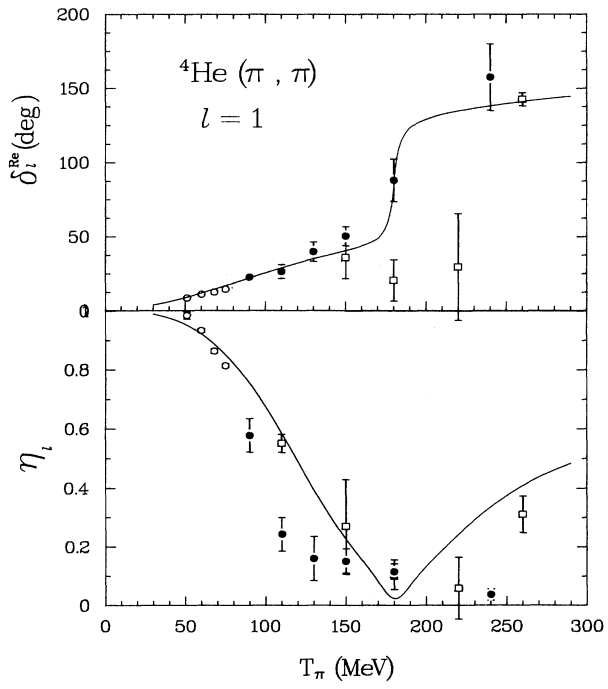

FIG. 8. Same as Fig. 9 but for $l = 1$.

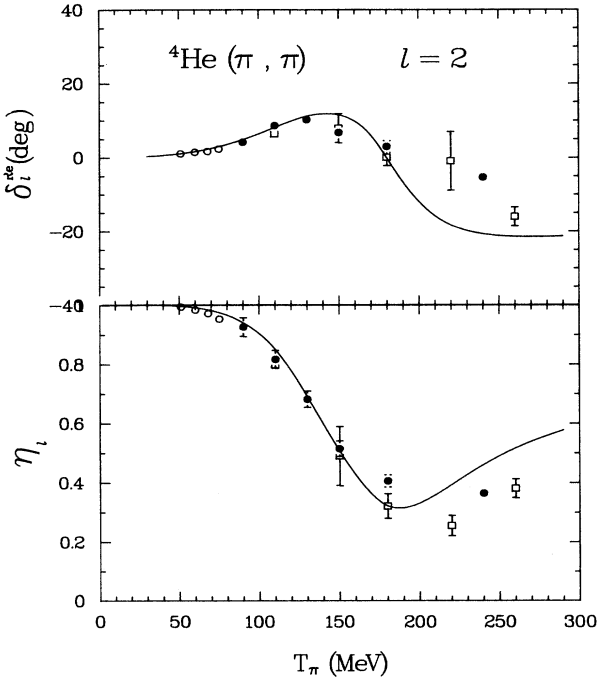

FIG. 9. Same as Fig. 9 but for $l = 2$.

of the energy-shifted optical model calculations. The effect of the π-nucleon P_{33} resonance is clearly visible in the energy dependences of all measured and calculated π-nucleus phases. When the energy shift is used, the strong energy dependence in δ_l^{Re} and the minimum in η_l occur at approximately the energies where they are observed in the experimental phase shifts. The experimental phase shifts show a more gradual change of δ_l^{Re} and η_l for the $l = 0$, 1, and 2 partial waves than the optical model predicts. It is worth noting that the experimental η_l for $l = 0$, 1, and 2 represent more absorption at $T_\pi = 240$ than at $T_\pi = 180$ MeV and much more absorption than the optical model calculation.

C. Forward-scattering amplitudes and dispersion relation prediction

The forward amplitude can be obtained by extrapolating the phase-shift fit to 0°. We calculated total nuclear cross sections from the imaginary part of the forward-scattering amplitude $\mathrm{Im}f_0$, using the optical theorem,

$$\sigma_{\mathrm{tot}} = \frac{4\pi}{k}\,\mathrm{Im}f_0. \tag{4}$$

The resulting values of σ_{tot} (Fig. 10) are mostly in agreement with the measured total nuclear cross sections of Wilkins *et al.* [35], averaged over π^+ and π^- scattering. At $T_\pi = 150$ MeV our value is below that of Ref. [35] at $T_\pi = 146$ MeV, but it agrees with that of Ref. [13] at 150 MeV. At $T_\pi = 110$ MeV the total nuclear cross section of Ref. [13] is lower than the values obtained both by Ref. [35] and from our phase-shift fit.

The optical model does quite well in predicting the total nuclear cross sections (Fig. 10). But the predicted width of the "P_{33}-resonance peak" is smaller than experimentally observed. Inclusion of Fermi motion in constructing the optical potential should lead to a smoother energy dependence of the partial waves and might resolve this discrepancy between the calculated and predicted total nuclear cross sections.

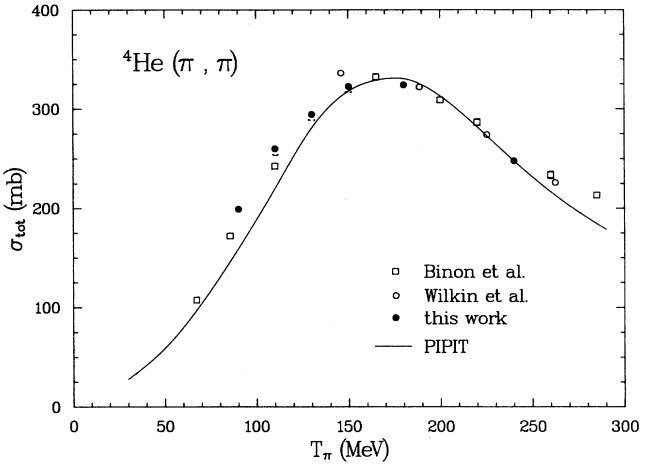

FIG. 10. Total nuclear cross section for π reactions with ^{4}He. The open circles are the measurements by Wilkins *et al.* [35] for the average of the total cross section obtained from π^+-^{4}He and π^--^{4}He. The open squares are from Binon *et al.* [13] from π^--^{4}He. The full circles are from the phase-shift analysis of this work. The solid line is the prediction of the optical model calculation.

The real part of the forward amplitude $\mathrm{Re}f_0$ extracted from the data is shown in Fig. 11. As the differential cross-section data indicated in the Coulomb-nuclear in-

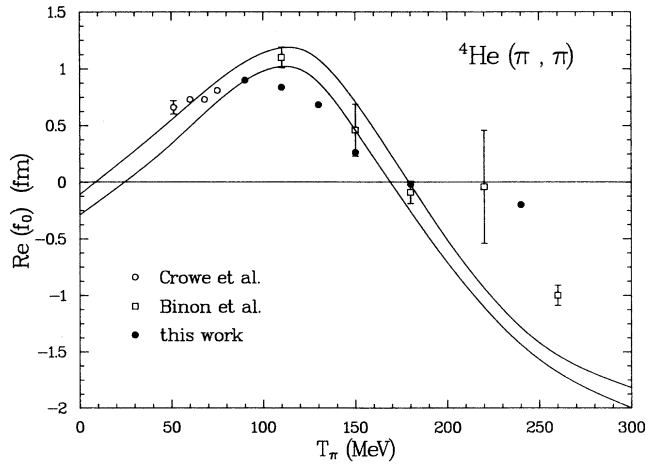

FIG. 11. Real part of the forward-scattering amplitude obtained from the phase-shift analysis. Solid dots: this work; open circles: results of Crowe *et al.* [11]; open squares: results of Binon *et al.* [13]. The full lines give the error band of the prediction of Grein and Locher [38] using the dispersion relation.

terference region, Ref_0 changes sign at about 180 MeV. As observed [13] and confirmed by our measurement at 240 MeV, there is a discrepancy between the real part of the forward amplitude at energies larger than T_π = 200 MeV and calculations using the forward dispersion relation [35] which links Ref_0 to Imf_0.

This discrepancy could be due to uncertainties in the knowledge of the total nuclear cross section. There are discrepancies of several standard deviations in the values of the total nuclear cross sections extracted by different groups [13, 35] at energies below T_π = 180 MeV. Furthermore, the total nuclear cross sections obtained from π^- + ^{4}He scattering are generally larger than those obtained from π^+ + ^{4}He scattering for energies below the resonance. This may be explained by the approximate treatment of Coulomb effects in the extraction of the nuclear cross sections. Wilkins *et al.* [35] showed that the inclusion of Coulomb barrier effects and trajectory distortions as suggested by Fäldt and Pilkuhn [36] can explain the larger cross section for π^-. Thus use of total nuclear cross sections extracted from π^- scattering without Coulomb correction leads to a systematic error in the application of the dispersion relation.

It has been suggested [31] that the lack of agreement with the forward dispersion relation above resonance energies is due to this uncertainty in the knowledge of the total cross section and the need to extrapolate the amplitudes into the unphysical region below threshold (to be able to use the dispersion relation). Indeed, Nichitiu *et al.* [31] succeeded in removing the discrepancy by using a new extrapolation procedure for the imaginary part of the amplitude to energies below threshold [14]. However, the slope of Imf_0 at threshold obtained in that analysis was found to be incompatible with data from mesic atoms [37].

In another analysis, Grein and Locher[38] concluded that uncertainties in the total cross section below resonance cannot explain the discrepancies at higher energies, because Ref_0 at energies above the P_{33} resonance is not sensitive enough to changes in Imf_0 at energies below the resonance. Instead they suggested that there might be a problem with the experimental total nuclear cross sections at higher energies.

It is presently not possible to draw definite conclusions from the discrepancy between Ref_0 from the forward dispersion relation and Ref_0 from the measurement of the elastic ^{4}He(π, π) differential cross sections. The situation might change when a new energy dependent phase-shift analysis is made, using a better treatment of Coulomb effects. Such an analysis could rely mainly on the Coulomb-nuclear interference in the elastic cross section to separate the real and imaginary parts of the forward amplitude. More high-quality elastic-scattering data at energies above the resonance will be needed for such an analysis.

IV. SUMMARY

We have measured differential cross sections for ^{4}He(π, π) elastic scattering for both π^+ and π^- at several energies spanning the region of the P_{33} resonance. The angular range included the region of Coulomb-nuclear interference as well as far backward angles. Fits to the data yielded phase shifts which vary less strongly with energy than predicted by a first-order optical model. Calculations of the real part of the forward amplitude based on the forward dispersion relation are in disagreement with the measurements at energies above the P_{33} resonance. The quality of the data should allow a thorough study of higher-order terms in the optical potential in future analyses.

ACKNOWLEDGMENTS

The authors are indebted to Dr. M. A. Franey and Prof. D. Ernst for useful discussions. This work was supported in part by the U.S. Department of Energy and the Robert A. Welch Foundation.

[a] Present address: Universität Karlsruhe, D 7500 Karlsruhe, Germany.
[b] Present address: Mission Research, Santa Barbara, CA 93109.
[c] Present address: Rutgers University, Piscataway, NJ 08855.
[d] Present address: CEBAF, Newport News, VA 23606.
[e] Present address: LAMPF, Los Alamos National Laboratory, Los Alamos, NM 87545.
[f] Present address: George Washington University, Washington, D.C. 20052.
[g] Permanent address: Ben-Gurion University of the Negev, Beer-Sheva, Israel.
[h] Present address: University of Pennsylvania, Philadelphia, PA 19104.
[i] Present address: Indiana University, Bloomington, IN 47405.

[1] W. R. Gibbs *et al.*, Phys. Rev. C **13**, 2433 (1976).
[2] L. S. Celenza, L. C. Liu, and C. M. Shakin, Phys. Rev. C **13**, 2451 (1976).
[3] T. S. Lee, Phys. Lett. **67B**, 282 (1977); T. S. Lee and S. Chakravarti, Phys. Rev. C **16**, 273 (1977).
[4] R. H. Landau and A. W. Thomas, Nucl. Phys. **A302**, 461 (1978).
[5] H. Garcilazo, Nucl. Phys. **A302**, 493 (1978).
[6] M. Wakamatsu, Nucl. Phys. **A312**, 427 (1978).
[7] R. Mach and M. G. Sapozhnikov, J. Phys. G **10**, 147 (1984).
[8] A. W. Thomas and R. H. Landau, Phys. Rep. **58**, 121 (1980).
[9] I. Sick, Phys. Lett. **116B**, 212 (1982).
[10] M. E. Nordberg, Jr., and K. F. Kinsey, Phys. Lett. **20**, 692 (1966).
[11] K. M. Crowe, A. Fainberg, J. Miller, and A. S. L. Parsons, Phys. Rev. **180**, 1349 (1969).
[12] G. Fournier *et al.*, Nucl. Phys. **A426**, 542 (1984).
[13] F. Binon *et al.*, Nucl. Phys. **A298**, 499 (1978).
[14] Yu. A. Shcherbakov *et al.*, Il Nuovo Cimento **31A**, 249

(1976).
[15] J. Källne *et al.*, Phys. Rev. Lett. **45**, 517 (1980).
[16] J. Boswell *et al.*, Nucl. Phys. **A466**, 458 (1987).
[17] H. A. Thiessen and S. Sobottka, Los Alamos National Laboratory Report LA-4534-MS, 1970 (unpublished).
[18] G. R. Burleson *et al.*, Nucl. Instrum. Methods **A247**, 327 (1986).
[19] C. L. Blilie, Ph.D. thesis, University of Minnesota, 1985 (unpublished).
[20] R. A. Arndt, Phase-shift set of 1990 from program SAID (unpublished).
[21] Field map performed by S. Archuletta.
[22] R. A. Eisenstein and F. Tabakin, Comput. Phys. Commun. **12**, 237 (1976).
[23] R. H. Landau, S. C. Phatak, and F. Tabakin, Ann. Phys. (N.Y.) **78**, 299 (1973).
[24] W. R. Cottingame and D. B. Holtkamp, Phys. Rev. Lett. **45**, 1828 (1980).
[25] J. A. Carr and F. Petrovich, program ALLWORLD (unpublished).
[26] S. Sterbenz, program UNFOLD (unpublished).
[27] C. W. de Jager, H. de Vries, and C. de Vries, At. Data Nucl. Data Tables **14**, 480 (1974).
[28] M. K. Jones, Ph.D. thesis, University of Minnesota, 1989 (unpublished).
[29] D. R. Giebink and D. J. Ernst, Comput. Phys. Commun. **48**, 407 (1988); D. J. Ernst, private communication.
[30] R. Mach, private communication.
[31] F. Nichitiu, I. V. Falomkin, M. G. Sapozhnikov, Yu. A. Shcherbakov, and P. Piragino, Il Nuovo Cimento **67A**, 1 (1982).
[32] M. Kh. Khankhasayev, F. Nichitiu, and M. G. Sapozhnikov, Czech. J. Phys. **B36**, 248 (1986).
[33] F. James and M. Roos, Comput. Phys. Commun. **10**, 343 (1975).
[34] F. Nichitiu and M. G. Sapozhnikov, Yad. Fiz. **37**, 1209 (1983) [Sov. J. Nucl. Phys. **37**, 718 (1983)].
[35] C. Wilkins *et al.*, Nucl. Phys. **B62**, 61 (1973).
[36] C. Fäldt and H. Pilkuhn, Phys. Lett. **46B**, 337 (1973).
[37] H. Pilkuhn, N. Zovko, and H. G. Schlaile, Z. Phys. A **279**, 293 (1976).
[38] W. Grein and M. P. Locher, J. Phys. G **6**, 653 (1980).